J. Fluid Mech. (2008), *vol.* 603, *pp.* 305–329.
doi:10.1017/S0022112008000931 Printed in the United Kingdom

Shallow-water modons on the f-plane

Z. KIZNER[1,2]†, G. REZNIK[3], B. FRIDMAN[2], R. KHVOLES[2] AND J. McWILLIAMS[4]

[1]Department of Physics, Bar-Ilan University, Ramat-Gan 52900, Israel

[2]Department of Mathematics, Bar-Ilan University, Ramat-Gan 52900, Israel

[3]P.P. Shirshov Institute of Oceanology, 36 Nakhimovsky Prosp., Moscow 117997, Russia

[4]Department of Atmospheric and Oceanic Sciences and Institute of Geophysics and Planetary Physics, University of California, Los Angeles 405 Hilgard Avenue Los Angeles, CA 90095-1565, USA

(Received 11 November 2007 and in revised form 3 February 2008)

Solutions for steadily translating localized vortical structures, or modons, are sought in the framework of a 1½-layer rotating shallow-water (RSW) model on the f-plane. In this model, the fluid is assumed to rotate at a constant rate and to be composed of an active finite-depth layer and a passive infinitely deep layer. The focus is on the smooth intense modons, in which the potential vorticity field is continuous, and the pressure (hence, the active-layer thickness) and velocity are smooth, while inertial effects and deviations of the active-layer thickness from the static level are considerable. The problem is solved numerically employing a Newton–Kantorovich iterative procedure, Fourier–Chebyshev spectral expansion and collocations. The numerics are preceded by a theoretical modon design discussion that includes: derivation of fundamental modon invariants; distinction between the flow in the trapped-fluid region and the flow outside it; and the boundary conditions at the separatrix, the streamline demarcating the two regions. Also, some basic distinctions from the quasi-geostrophic modons are discussed, and an asymptotic analysis of the RSW modon far-field characteristics is carried out. This analysis reveals that an RSW modon must propagate more slowly than inertia–gravity waves. In smooth modons, the requirement that the active-layer thickness should be positive imposes an even stronger restriction on the allowed translational speed. To enable the use of Fourier–Chebyshev series, only the modons with circular separatrices are considered. The numerical iterative procedure is initialized by an analytical quasi-geostrophic dipolar modon solution; accordingly, the obtained RSW modons appear as cyclone–anticyclone pairs. Computations show that the allowed maximal translational speed monotonically decreases as a function of the modon size and, for reasonable sizes, is appreciably smaller than the gravity-wave limit. As distinct from quasi-geostrophic modons, the RSW modons with circular separatrices display nonlinearity of the potential vorticity (PV) *vs.* streamfunction relation, and the cyclone–anticyclone asymmetry: while the integral mass anomaly in the modon is zero, the cyclone is more intense and compact than the anticyclone.

1. Introduction

We use the term 'modon' (introduced by Stern 1975) to designate localized vortices that propagate steadily without changing their parameters. Anti-symmetric dipoles in two-dimensional flows represent a classical example of a modon. The first solution

† Author to whom correspondence should be addressed: zinovyk@mail.biu.ac.il

that (using the contemporary terminology) can be categorized as a modon was suggested independently by Lamb (1895) and Chaplygin (1903). This is the well-known translating circular dipole solution to the Euler equations in two dimensions. The interest in this solution was rekindled in the 1970s (when the wide-ranging work on mesoscale, or synoptic, oceanic eddies started) after the modon publications of Stern (1975) and Larichev & Reznik (1976*a*, *b*) have appeared. During the past three decades, considerable progress has been made in developing the modon theory applied to plasma and geophysical (rotating and stratified) fluids.

Until now, the modons were studied using the quasi-geostrophic (QG) approximation, which is based on two assumptions: the deviation of isopycnal surfaces (or, alternatively, of the layer interfaces in a layered model) from their static states is small; and the Rossby number (which characterizes the magnitude of the nonlinear inertial forces relative to the Coriolis force) is also small (Pedlosky 1987). In the QG approximation, the equations of momentum conservation and continuity can be reduced to one equation of the potential vorticity (PV) conservation. If at least one of the above conditions is violated, more complex models should be used, the 1½-layer rotating shallow-water (RSW) model being one of them. Within this model, the fluid is assumed to be composed of two layers of different densities, one of the layers being infinitely deep and, therefore, passive. In oceanographic or meteorological applications, the active layer is the upper or the lower layer, respectively. It is essential that, in the rotating shallow-water model, the variation in the thickness of the active layer is allowed to be comparable to the layer thickness itself. Therefore, although the horizontal velocity components are assumed depth-independent in the RSW model, the variations of the active-layer thickness can be significant in the mass conservation. A barotropic interpretation of the same model is a single fluid layer whose thickness can vary significantly owing to the change in the free-surface elevation.

When a travelling modon is considered in a co-moving frame of reference, two areas can naturally be distinguished, the interior (or trapped-fluid) region where the streamlines are closed, and the exterior region where they are open (Larichev & Reznik 1976*a*; Flierl *et al.* 1980). The closed streamline that demarcates the two regions is conventionally termed the modon separatrix. Although, in any steady-state flow, PV and the streamfunction are functionally related, markedly, in travelling modons, the functionals are different for the exterior and interior regions (Larichev & Reznik 1976*a*). Accordingly, in the above-referenced analytical modon solutions where the separatrix is a circle, the exterior and interior flows are derived separately with their subsequent matching at the separatrix. This tactic proves to be beneficial also when searching for non-circular modons by numerical methods (for discussion see, Kizner, Berson & Khvoles 2003*a*; Khvoles, Berson & Kizner 2005). The pressure and velocity fields are required to be continuous, whereas PV (which is conserved by any fluid particle) can be discontinuous at the separatrix, because the PV values calculated from outside and inside, while being constant at the separatrix, need not necessarily be equal. In many cases, by special fitting of the modon parameters, the continuity of PV can also be achieved. The localization of a modon implies that its kinetic momentum, energy, etc. are finite; thus, a modon solution is characterized by a sufficiently fast decrease of the flow characteristics at infinity, i.e. with increasing distance from the separatrix.

Under the rigid-lid condition, that is, when the free-surface elevation is negligible, the Lamb–Chaplygin solution remains valid on a barotropic f-plane, where the Coriolis parameter f associated with the fluid rotation is constant. The barotropic solutions of Stern (1975) and Larichev & Reznik (1976*a*, *b*) are valid on the β-plane, where the gradient β of the Coriolis parameter is assumed to be constant. The first of

these solutions represents a standing dipole under the rigid-lid condition, whereas the second is a free-surface translating modon. In travelling β-plane and free-surface (or 1½-layer) f-plane QG modons, the decrease of the modon characteristics at infinity is exponential; thus the localization is truly high. Inspired by the works of Stern and Larichev & Reznik, a number of exact and asymptotic barotropic solutions were suggested, describing travelling modons on the f- and β-planes and in spherical geometry (Larichev & Reznik 1976*b*; Berestov 1981; Verkley 1984, 1987; Tribbia 1984; Nycander 1988). Several publications were devoted to numerical construction of barotropic modon solutions (Boyd & Ma 1990; Haupt, McWilliams & Tribbia 1993; Verkley 1993; Khvoles *et al.* 2005). Laboratory experiments show that circular modon solutions describe adequately some weak dipole flows produced in a fast rotating fluid (e.g. Flierl, Stern & Whitehead 1983; Flór & van Heijst 1994), although numerical simulations (Kizner *et al.* 2002, 2003*a*; Khvoles *et al.* 2005) and recent laboratory experiments (unpublished) suggest that modons with elliptical separatrices can be of practical interest.

Apart from Stern's dipole, standing β- and f-plane antisymmetric dipolar vortical solutions were suggested by Hesthaven *et al.* (1995) and Khvoles *et al.* (2005). In fact, to balance the self-propulsion natural in vortex pairs, such a dipole must possess some abnormal qualities (which probably explains why emergence of standing dipoles was never observed in simulations or laboratory experiments, Khvoles *et al.* 2005). In Stern's β-plane circular solution and in the standing elliptical β-plane solution of Khvoles *et al.* (2005), this is the vorticity jump across the dipole edge (related to the absence of flow outside the dipole). The peculiarity of the f-plane modon of Hesthaven *et al.* (1995), in which the uniqueness of the PV *vs.* streamfunction relation is postulated, is in the absence of a separatrix and the existence of unlimited areas enclosing the dipole, where the vorticity is oppositely signed. That is, in terms of vorticity, unlike the Lamb–Chapygin modon, the modon of Hesthaven *et al.* is not confined to a finite-size area. Modons of both Stern and Hesthaven *et al.* were shown to be strongly unstable (Kizner & Berson 2000; Hesthaven *et al.* 1995). All these explain our special interest in translating modons.

Along with barotropic modons, several explicit baroclinic QG modon solutions – analytical, asymptotic, and numeric – have been proposed (Berestov 1979; Flierl *et al.* 1980; Kizner 1984, 1986*a*, *b*, 1988, 1997; Neven 1994; Pakyari & Nycander 1996; Reznik & Sutyrin 2001; Kizner *et al.* 2003*b*; Khvoles, McWilliams & Kizner 2007). The first two-layer QG modon solutions on the β-plane were suggested by Flierl *et al.* (1980). These are the so-called modon-with-a-rider constructions with a PV jump across the separatrix. Such a solution appears as a sum of a barotropic Larichev–Reznik dipole and a circularly symmetric baroclinic monopole (rider). The addition of a rider makes the flow in each layer asymmetric about the axis of the modon translation. Flierl *et al.* (1980) considered also barotropic solutions of this kind; as discovered by Meleshko & van Heijst (1994), the first barotropic dipole-plus-monopole vortical solution was suggested by Chaplygin (1903). Kizner (1984) suggested smooth quasi-geostrophic baroclinic β-plane solutions of the modon-with-a-rider type marked by continuity of the PV field. These solutions can bear any baroclinic mode (or a number of baroclinic modes) and can be fitted to any density stratification, both continuous and multi-layer, thus being relevant to mesoscale eddies observed in the ocean and atmosphere (Kizner 1997; for application to intra-thermocline vortices see Kizner *et al.* 2002). Importantly, an anti-symmetric barotropic dipole modon is always smooth in the above sense, whereas PV in a barotropic modon-with-a-rider solution is necessarily discontinuous. Baroclinicity renders an extra degree of freedom

to a modon solution, because the constant value assumed by a baroclinic mode of the co-moving streamfunction at the separatrix, in general, can be set arbitrarily. Special fitting of this constant enables the construction of smooth baroclinic solutions, i.e. those with continuous PV (Kizner *et al.* 2003*a*,*b*; Khvoles *et al.* 2007). As will be seen below, this idea is feasible not only in the QG framework. Based on numerical evidence, PV continuity appears to be essential for the modon stability: whereas smooth modons prove to be quite robust, all known modon solutions (whether barotropic or two-layer) with vorticity jumps across separatrices are strongly unstable (Swenson 1987; Kizner & Berson 2000; Kizner *et al.* 2003*a*; Khvoles *et al.* 2005).

As the above brief review implies, during the past three decades, the theory of modons in the QG approximation has been developed extensively. However, no theoretical work devoted to ageostrophic modons has been carried out so far. There is only some preliminary numerical (Konshin & Shapiro 1988; Pallas-Sanz & Viudez 2007) and experimental (Sous, Bonneton & Sommeria 2004) indication of the possibility of existence of ageostrophic modons.

Our paper is devoted to clarification of the question of the existence of RSW modons on the f-plane. We provide analytical arguments in favour of the existence of localized steadily translating vortical structures; present a numerical algorithm aimed at the construction of explicit (steady-state) RSW modon solutions; and, using this algorithm, produce a broad spectrum of RSW modons. The numerical algorithm, which is based on a Newton–Kantorovich successive-linearization procedure supplemented with Fourier–Chebyshev approximation of the solution and collocation, allows construction of the modon solutions at quite a good accuracy. First, the solution outside the separatrix is constructed and the boundary conditions for the interior problem are established; thereafter, the interior solution is found. To enable the Fourier expansion in the azimuth angle, we assume the separatrix to be a circle. As with the baroclinic component in two-layer QG modons, the constant streamfunction value at the separatrix can be set arbitrarily, while special fitting of this constant provides modons with continuous PV fields. Such modons constitute a two-parameter family, the parameters being the separatrix radius L and the modon's translational speed U. Like QG modons, the simplest RSW modon is a pair cyclone–anticyclone. The ageostrophicity in smooth modons is apparent primarily in the cyclone–anticyclone asymmetry, the cyclone being more compact and having a stronger peak PV than the anticyclone. With increasing U and L this asymmetry enhances, the minimal thickness of the active layer (in the cyclone centre) decreases, and the cyclone peak PV increases. The requirement that the thickness of the active layer in the cyclone must be positive imposes a constraint on parameters U and L.

In § 2, the theoretical background is provided, including the basic equations and the energy and PV invariants. The main principles underlying the construction of RSW modons and the equations and boundary conditions for the exterior and interior regions are discussed in § 3. In this section, we also present the circular QG modon which serves as a prototype for RSW modons. Asymptotic considerations presented in § 3 testify in favour of the existence of highly localized steadily translating vortical structures (i.e. two-dimensional solitons) in the RSW approximation. In § 4, the numerical algorithm is described. The modon solutions resulting from our computations are presented and discussed in § 5. The main results are summarized in § 6.

2. Theoretical background

2.1. *Steady-state equations*

Consider a two-layer fluid rotating at a constant angular velocity Ω. One of the layers (say, the lower one) is assumed to be infinitely deep, hence passive. The motion in the active (upper) layer is assumed to be hydrostatic, and the horizontal velocities to be depth independent. The governing equations of this model are:

$$\frac{\partial u}{\partial t} + u\frac{\partial u}{\partial x} + v\frac{\partial u}{\partial y} - fv + g'\frac{\partial h}{\partial x} = 0, \tag{1}$$

$$\frac{\partial v}{\partial t} + u\frac{\partial v}{\partial x} + v\frac{\partial v}{\partial y} + fu + g'\frac{\partial h}{\partial y} = 0, \tag{2}$$

$$\frac{\partial h}{\partial t} + \frac{\partial}{\partial x}(uH) + \frac{\partial}{\partial y}(vH) = 0. \tag{3}$$

Here, u and v are the x- and y-components of velocity; $f = 2\Omega = \text{const}$ is the Coriolis parameter (the f-plane approximation); $H = H_0 + h$ is the active-layer thickness, H_0 and h being the mean thickness and the deviation from it; and g' is the reduced gravity (i.e. the acceleration due to gravity multiplied by the density jump between the layers, divided by the lower-layer density). This model is known as the 1½-layer RSW, or reduced gravity approximation.

We are searching for modons, i.e. highly localized vortex structures that translate steadily without any change in their characteristics. For definiteness we assume that a modon travels along the $x-$axis at a constant speed U, so that the variables u, v and h are functions of $x - Ut$ and y only. Thus, in a co-moving frame of reference, the flow is stationary and obeys the equations:

$$(u-U)\frac{\partial u}{\partial x} + v\frac{\partial u}{\partial y} - fv + g'\frac{\partial h}{\partial x} = 0, \tag{4}$$

$$(u-U)\frac{\partial v}{\partial x} + v\frac{\partial v}{\partial y} + fu + g'\frac{\partial h}{\partial y} = 0, \tag{5}$$

$$\frac{\partial}{\partial x}[(u-U)H] + \frac{\partial}{\partial y}(vH) = 0. \tag{6}$$

2.2. *Energy and potential vorticity conservation*

Although, according to (3), the flow in the RSW model is generally divergent or convergent, for a steady-state flow considered in the co-moving frame of reference, (6) allows the introduction of a co-moving streamfunction Ψ:

$$(u-U)H = -\frac{\partial \Psi}{\partial y}, \qquad vH = \frac{\partial \Psi}{\partial x}. \tag{7}$$

Thus, the energy and potential vorticity conserved in each fluid column confined in the active layer are functions of Ψ. It can easily be verified that these functions are related to each other (Malanotte-Rizzoli 1982):

$$B = \frac{(u-U)^2}{2} + \frac{v^2}{2} + g'h + Ufy = F(\Psi), \tag{8}$$

$$P = \frac{\zeta + f}{H} \equiv Q + \frac{f}{H_0} = \frac{\mathrm{d}F(\Psi)}{\mathrm{d}\Psi}, \quad Q = \frac{1}{H_0 + h}\left(\zeta - \frac{f}{H_0}h\right). \tag{9}$$

Here, B is the Bernoulli function (also referred to as energy); P is the PV; $F(\Psi)$ is some (unknown at the moment) differentiable function of Ψ, and

$$\zeta = \frac{\partial v}{\partial x} - \frac{\partial u}{\partial y} \tag{10}$$

is the relative vorticity.

Using (7)–(10), variables B and Q can be expressed in terms of Ψ, and h as

$$B = \frac{1}{2H^2}\left[\left(\frac{\partial \Psi}{\partial x}\right)^2 + \left(\frac{\partial \Psi}{\partial y}\right)^2\right] + g'h + Ufy, \tag{11}$$

$$Q = \frac{\Delta \Psi}{H^2} - \frac{1}{H^3}\left(\frac{\partial h}{\partial x}\frac{\partial \Psi}{\partial x} + \frac{\partial h}{\partial y}\frac{\partial \Psi}{\partial y}\right) - \frac{f}{H_0}\frac{h}{H}, \tag{12}$$

where Δ is the Laplacian operator in two dimensions. The existence of functional relations between Q and B, on the one hand, and Ψ, on the other (see (8) and (9)), implies the following equations:

$$J(\Psi, B) = 0, \tag{13}$$

$$J(\Psi, Q) = 0, \tag{14}$$

where J is the Jacobian operator. Note that the reverse assertion is false: generally, (13) and (14) do not imply (8) and (9) and, hence, (4)–(6), because they do not guarantee that $\mathrm{d}B(\Psi)/\mathrm{d}\Psi = P(\Psi)$.

2.3. *Null integral mass anomaly in a modon*

In addition to the above-listed characteristics of steadily translating RSW flows, a modon must have a zero integral mass anomaly. To prove this statement, we multiply both parts of (4) and of (6) by H and u, respectively, and sum the results to obtain:

$$-U\frac{\partial (Hu)}{\partial x} + \frac{\partial (Hu^2)}{\partial x} + \frac{\partial (Huv)}{\partial y} - fHv + g'H\frac{\partial h}{\partial x} = 0. \tag{15}$$

In a similar way, an analogous equation is obtained from (5) and (6):

$$-U\frac{\partial (Hv)}{\partial x} + \frac{\partial (Huv)}{\partial x} + \frac{\partial (Hv^2)}{\partial y} + fHu + g'H\frac{\partial h}{\partial y} = 0. \tag{16}$$

Eliminating h from (15), (16) by cross-differentiation and using (6) yields:

$$-U\frac{\partial}{\partial x}\left[\frac{\partial (Hv)}{\partial x} - \frac{\partial (Hu)}{\partial y}\right] + fU\frac{\partial h}{\partial x} + \frac{\partial^2 (Huv)}{\partial x^2} - \frac{\partial^2 (Huv)}{\partial y^2} - \frac{\partial^2 [H(u^2 - v^2)]}{\partial x \partial y} = 0. \tag{17}$$

Multiplication of (17) by x and integration over the plane, under the condition that u, v and h and their first derivatives go to zero at infinity faster than $1/r^2$, results in the following equation:

$$\int h \mathrm{d}x\, \mathrm{d}y = 0. \tag{18}$$

Equation (18) means that the total mass anomaly in an RSW modon must be zero. In this sense, RSW modons are no different from QG modons (e.g. Flierl *et al.* 1980).

2.4. *Non-dimensionalization*

All explicit modon solutions suggested up to now fall into the category of QG modons. As will be demonstrated below (§§ 4 and 5), by using a computational continuation approach, we produce modon solutions that cover the whole spectrum

of the RSW model parameters. In so doing, we start with QG modons as beginnings of sequences of solutions that end in the sought-for ageostrophic modons. To establish the transition from a QG regime to the RSW balance, it is expedient to present the equations of §§ 2.1 and 2.2 in a non-dimensional form. Let the modon translation speed U be the velocity scale; $h^* = LfU/g'$, the scale for the deviation h of the active-layer thickness (found via the assumption that the Coriolis acceleration and that due to the gradient of h are of the same order of magnitude); and the modon radius L, the horizontal length scale. In such non-dimensional variables, (4)–(6) become:

$$Ro\left[(u-1)\frac{\partial u}{\partial x} + v\frac{\partial u}{\partial y}\right] - v + \frac{\partial h}{\partial x} = 0, \tag{19}$$

$$Ro\left[(u-1)\frac{\partial v}{\partial x} + v\frac{\partial v}{\partial y}\right] + u + \frac{\partial h}{\partial y} = 0, \tag{20}$$

$$\varepsilon\left[(u-1)\frac{\partial h}{\partial x} + v\frac{\partial h}{\partial y}\right] + (1+\varepsilon h)\left(\frac{\partial u}{\partial x} + \frac{\partial v}{\partial y}\right) = 0, \tag{21}$$

where the previous notations are retained for the non-dimensional variables. The non-dimensional parameters appearing in (19)–(21) are:

$$\varepsilon = \frac{h^*}{H_0}, \quad Ro = \frac{U}{Lf} = \frac{1}{\Lambda^2}\varepsilon, \quad \Lambda = \frac{L}{L_R}, \tag{22}$$

where Λ is the modon radius relative to the Rossby deformation radius $L_R = \sqrt{g'H_0}/f$, so that $1/\Lambda^2$ is the Burger number. According to (22), the Rossby number Ro and the typical relative variation of the layer thickness, ε, are proportional to each other with the factor of proportionality, the Burger number, being a function of the modon size. The non-dimensional layer thickness, $H = 1 + \varepsilon h$, must be positive; otherwise the problem set-up becomes unphysical and mathematically incomplete. This restriction imposes some constraint on the modon parameters discussed in § 5.

Once the length, thickness variation, and velocity scales are specified as L, h^* and U, the scales for Ψ, B and P become UH_0L, UfL and f/H_0, respectively. In non-dimensional variables defined in this way, equations (10), (13), and (14) remain unchanged, whereas (7)–(9), (11) and (12) convert into

$$(u-1)(1+\varepsilon h) = -\frac{\partial \Psi}{\partial y}, \quad v(1+\varepsilon h) = \frac{\partial \Psi}{\partial x}, \tag{23}$$

$$B = Ro\left[\frac{(u-1)^2}{2} + \frac{v^2}{2}\right] + h + y = \frac{Ro}{2}\frac{1}{(1+\varepsilon h)^2} \times \left[\left(\frac{\partial \Psi}{\partial x}\right)^2 + \left(\frac{\partial \Psi}{\partial y}\right)^2\right] + h + y = F(\Psi), \tag{24}$$

$$P = RoQ + 1 = \frac{\mathrm{d}F(\Psi)}{\mathrm{d}\Psi}, \tag{25}$$

$$Q = \frac{1}{1+\varepsilon h}(\zeta - \Lambda^2 h) = \frac{\Delta \Psi}{(1+\varepsilon h)^2} - \varepsilon\frac{1}{(1+\varepsilon h)^3}\left(\frac{\partial h}{\partial x}\frac{\partial \Psi}{\partial x} + \frac{\partial h}{\partial y}\frac{\partial \Psi}{\partial y}\right) - \Lambda^2\frac{h}{1+\varepsilon h}. \tag{26}$$

Below, we deal with the non-dimensional variables unless otherwise stated.

3. RSW modon design

3.1. *Quasi-geostrophic modon prototype*

Localization of a modon means that, as $x, y \to \infty$, variables u, v, h go to zero fast enough to guarantee finiteness of the modon energy. Accordingly, $\Psi \to y$ as $x, y \to \infty$. The latter implies that, at infinity, the flow considered in the co-moving frame of reference tends to a uniform flow with the non-dimensional velocity -1 along the x-axis. For the sake of asymptotic analysis, it is convenient to represent Ψ as a superposition

$$\Psi = \psi + y, \tag{27}$$

where the streamfunction anomaly ψ is supposed to vanish at infinity.

The QG regime is obtained as $Ro \to 0$ and $\varepsilon \to 0$ at a fixed Λ. As may be seen from (19), (20) and (27), in the QG limit the flow is non-divergent, and $h = \psi$ is the streamfunction for the (u, v)-flow. In this limit, according to (23), $B = h + y = \psi + y = \Psi$, so that relation (13) becomes trivial, whereas (26) implies:

$$Q = \Delta\Psi - \Lambda^2 h = \Delta h - \Lambda^2 h = \Delta\psi - \Lambda^2\psi. \tag{28}$$

The simplest QG modon solution to (14), (27) and (28) is based on the assumption that Q is zero outside a circle of radius 1 and is proportional to Ψ inside it with a negative coefficient of proportionality $-A^2$:

$$\Delta\psi - \Lambda^2\psi = \begin{cases} -A^2(\psi + y), & r < 1, \\ 0, & r \geqslant 1. \end{cases} \tag{29}$$

The corresponding solution written in non-dimensional variables is:

$$\psi = h = \begin{cases} \left[\dfrac{\Lambda^2}{\Pi^2}\dfrac{J_1(\Pi r)}{J_1(\Pi)} - r\left(1 + \dfrac{\Lambda^2}{\Pi^2}\right)\right]\sin\theta, & r < 1, \\ -\dfrac{K_1(\Lambda r)}{K_1(\Lambda)}\sin\theta, & r \geqslant 1. \end{cases} \tag{30}$$

In (29) and (30), r and θ are the polar coordinates, J_1 and K_1 are the first-order Bessel and Macdonald (modified Bessel) functions, and $\Pi = \sqrt{A^2 - \Lambda^2}$. Solution (30) suggested by Larichev & Reznik (1976*a*, *b*) for a free-surface QG β-plane is reproduced here in the particular case of $\beta = 0$ (see also Reznik 1992). In substance, (29) is an eigenvalue problem with a countable spectrum of eigenvalues $-\Pi^2$. Given Λ, the spectrum of Π (and, therefore, A) values is determined by the so-called modon dispersion relation that secures the continuity of $\psi = h$ and their first derivatives at $r = 1$:

$$\frac{\Pi J_1(\Pi)}{J_2(\Pi)} = -\frac{\Lambda K_1(\Lambda)}{K_2(\Lambda)}, \tag{31}$$

(here J_2 and K_2 are the second-order Bessel and Macdonald functions). The solution based on the smallest root of (31) represents a dipolar modon. In terms of dimensional ψ or h, the QG modon solution is obtained by multiplying the right-hand side of (30) by UH_0L or LfU/g', respectively, and replacing r with r/L, which implies the replacement of the inequalities $r < 1$ and $r \geqslant 1$ with $r < L$ and $r \geqslant L$. Thus, because $\Lambda = L/L_R$, this solution is determined by a pair of dimensional parameters U and L. Clearly, (30) and (31) can be interpreted as an approximate solution to the system of equations (4)–(6) at small Ro and ε. This is used in the numerical search for RSW modons (§4).

3.2. *Separatrix*

As noted above, because the modon is localized and propagates steadily, its far-field flow considered in a co-moving frame of reference is nearly uniform. Therefore, there must exist a separatrix Γ, a closed contour that demarcates the interior (or trapped-fluid) region where streamlines are closed, and the exterior region in which streamlines are open and go to straight lines as $r \to \infty$ (Larichev & Reznik 1976*a*; Flierl *et al.* 1980; Kizner 1997). In principle, the separatrix form can be set variously. In most of the QG modon solutions found so far, the separatrices are circular or elliptical (see § 1 for references). Just as in QG modons, the exterior and interior solutions for an RSW modon are constructed separately and are matched at the separatrix so as to guarantee the continuity of physically meaningful variables Ψ, u, v, h, B, and the first derivatives of h. In fact, satisfaction of part of these conditions affords the fulfilment of the remaining ones (see §§ 3.3.1 and 3.4). To minimize the number of free parameters of the problem and to allow the Fourier expansion in the azimuth angle θ, we shall follow the example considered in § 3.1, i.e. confine ourselves to the case of a circular separatrix of radius $r = 1$.

As with QG modons, function F in the exterior region of an RSW modon is specified uniquely by the asymptotics of (7)–(9) at $x \to \infty$; this provides the equations for the exterior domain. In the interior domain, function F can be different for different modon solutions (or, more specifically, for different ε, Λ, and the separatrix forms). Thus, in general, inside contour Γ, the solution should be described by (4) and (5) written in terms of Ψ and h. Handling of the exterior and interior regions is described in more detail in the next two sections.

3.3. *Exterior domain*

3.3.1. *Governing equations and boundary conditions*

In this section, all variables correspond to the exterior region, outside the separatrix. At infinity ($x \to \infty$), where the flow becomes uniform, $Q = 0$ and $B = y + Ro/2$ (this is because $u, v, h, \psi \to 0$, and $\Psi \to y$ as $x \to \infty$). Owing to the energy and PV conservation, along the open streamlines, functions B and Q must assume the same values as at infinity. Therefore, according to (24), the functional equation $y + Ro/2 = F(y)$ holds, meaning that, throughout the exterior region,

$$F(\Psi) = \Psi + \frac{1}{2}Ro. \tag{32}$$

Equations (24) and (32) yield:

$$\frac{Ro}{2}\left\{\frac{1}{(1+\varepsilon h)^2}(\nabla\Psi)^2 - 1\right\} - \Psi + h + y = 0, \tag{33}$$

while the condition $Q = 0$ combined with (26) implies:

$$\frac{\Delta\Psi}{1+\varepsilon h} - \varepsilon\frac{1}{(1+\varepsilon h)^2}\nabla h \cdot \nabla\Psi - \Lambda^2 h = 0. \tag{34}$$

It is readily verified that, in the exterior region, (23), (33) and (34) (and, therefore, (13) and (14)) are equivalent to (19)–(21). Thus, (33) and (34) supplemented with proper boundary conditions fully determine the exterior structure of the solution sought.

The boundary condition which the exterior solution must obey at the separatrix Γ is:

$$\Psi = C \quad \text{at} \quad r = 1, \tag{35}$$

where C is an arbitrary (for the moment) constant. The conditions at infinity are

$$\psi \to 0 \text{ (i.e. } \Psi \to y), \quad h \to 0 \quad \text{as} \quad r \to \infty. \tag{36}$$

Noticeably, as distinct from the QG limit (29), the system of equations and boundary conditions (33)–(36) for the exterior region is nonlinear and quite complex. Therefore, it is handled numerically. In so doing, (33) and (34) are written in polar coordinates, while parameter C is varied to find a solution with a continuous PV and smooth B fields.

3.3.2. *Asymptotics for* $r \to \infty$

Although we cannot prove rigorously the existence of solutions to the problem determined by (33)–(36), there are some solid arguments in favour of their existence. In § 5, we present a variety of modons found numerically. These solutions fall off at the periphery and satisfy (33)–(36) (as well as the equations and boundary conditions for the interior domain) at quite a high accuracy in a large bounded region $r \leqslant R$ (where $R \gg 1$). In § 5, we also discuss the limitations allowing the existence of smooth modons. At this juncture, to make certain that conditions (36) are, in principle, feasible, and to reveal the degree of localization of an RSW modon, we consider the asymptotic behaviour of the solutions for $r \to \infty$.

Assuming $\psi \to 0$ and $h \to 0$, (33) and (34) can be linearized to yield

$$Ro\left(\frac{\partial \psi}{\partial y} - \varepsilon h\right) - \psi + h = 0 \tag{37}$$

and

$$\Delta\psi - \varepsilon \frac{\partial h}{\partial y} - \Lambda^2 h = 0. \tag{38}$$

By employing (37), h can be expressed in terms of ψ. Substituting this expression in (38) we arrive at the following equation that describes the asymptotic behaviour of the modon solution at small h and ψ, or more specifically, far away from the separatrix (as $r \to \infty$):

$$\left(1 - \frac{\varepsilon^2}{\Lambda^2}\right)\frac{\partial^2 \psi}{\partial x^2} + \frac{\partial^2 \psi}{\partial y^2} - \Lambda^2 \psi = 0. \tag{39}$$

At $\varepsilon/\Lambda < 1$, by normalizing the x-coordinate with $\sqrt{1 - \varepsilon^2/\Lambda^2}$, (26) transforms into a Helmholtz equation that has solutions dying out exponentially as $r \to \infty$. At $\varepsilon/\Lambda > 1$, (39) becomes a telegraph (Klein–Gordon) equation that has no highly localized solutions.

Thus, a necessary condition for the existence of (exponentially) localized modon solutions is $\varepsilon/\Lambda \leqslant 1$ or, what is the same, $Ro\Lambda \leqslant 1$, or $Ro\varepsilon \leqslant 1$. In other words, this is a necessary condition for the existence of two-dimensional RSW solitons. In view of (22), this condition can be interpreted as a restriction on the (dimensional) translation speed of a modon:

$$U \leqslant \sqrt{g' H_0} \tag{40}$$

(because the modon is assumed to propagate in the x-direction, U is positive). Clearly, any one-dimensional soliton will obey condition (40) (Li 2004).

The physical meaning of constraint (40) becomes clear if we consider the spectrum of linear waves permitted in the RSW model (1)–(3). The spectrum consists of the inertia–gravity harmonic waves, $\exp[\mathrm{i}(kx + ly - \omega t)]$, obeying the following dispersion

relation between the frequency ω and wavenumbers k and l:

$$\omega = \pm\sqrt{(k^2+l^2)g'H_0 + f^2}. \tag{41}$$

The absolute value of the phase speed of an inertia-gravity wave is $|\omega|/\sqrt{k^2+l^2}$; its lower bound is reached in the short-wave limit, $k^2+l^2 \to \infty$, and is equal to $\sqrt{g'H_0}$ the phase speed of gravity waves. Equations (1)–(3) allow only one type of wave, inertia–gravity waves. In such systems, solitons can propagate at speeds that are outside the range of phase speeds of possible linear waves. This condition ensures that the localized structures do not radiate waves, thus remaining steady. In our case, (40) asserts that a highly localized vortical structure can be stationary in a co-moving frame of reference if it propagates at a speed different from the phase speeds of linear inertia–gravity waves. Note that the translation speed U of an f-plane QG modon (which is also highly localized) can be arbitrary since parameters Λ and Π do not depend on U (see (30) and (31)). This arbitrariness of U is related to the fact that the linearized QG version of (1)–(3), $(\partial/\partial t)(\nabla^2\psi - \Lambda^2\psi) = 0$, does not allow any waves. This is, by the way, an important difference of f-plane QG modons from β-plane QG modons: the latter are allowed to propagate only with speeds different from the phase speeds of Rossby waves.

3.4. *Interior domain and smooth solutions*

It can easily be shown that, under the condition $\mathrm{d}B/\mathrm{d}\Psi = P$, (13), (14) and (23) are equivalent to (19)–(22). However, when solving (13) and (14) in a given domain directly (by some numerical method), no additional functional condition of the above-mentioned type can be imposed on B and Q: the functionals relating B and Q to Ψ are determined *a posteriori*, i.e. once the solution to (13) and (14) is already found. Therefore, when dealing with the interior region, we have to employ the original equations (19), (20) and (23). In polar coordinates (which are used in computations) these equations convert into

$$\frac{Ro}{H}\left[\frac{\partial\Psi}{\partial r}\frac{\partial}{\partial\theta}\left(\frac{1}{H}\frac{\partial\Psi}{\partial r}\right) - \frac{\partial\Psi}{\partial\theta}\frac{\partial}{\partial r}\left(\frac{1}{H}\frac{\partial\Psi}{\partial r}\right) - \frac{1}{rH}\frac{\partial\Psi}{\partial r}\frac{\partial\Psi}{\partial\theta}\right] - \frac{1}{H}\frac{\partial\Psi}{\partial\theta} + r\cos\theta + \frac{\partial h}{\partial\theta} = 0, \tag{42}$$

$$\frac{Ro}{rH}\left[\frac{\partial\Psi}{\partial r}\frac{\partial}{\partial\theta}\left(\frac{1}{rH}\frac{\partial\Psi}{\partial\theta}\right) - \frac{\partial\Psi}{\partial\theta}\frac{\partial}{\partial r}\left(\frac{1}{rH}\frac{\partial\Psi}{\partial\theta}\right) + \frac{1}{H}\left(\frac{\partial\Psi}{\partial r}\right)^2\right] + \frac{1}{H}\frac{\partial\Psi}{\partial r} - \sin\theta - \frac{\partial h}{\partial r} = 0 \tag{43}$$

(for brevity, we use H for $1+\varepsilon h$).

Equations (42) and (43) for the interior domain are supplemented with the following boundary conditions at the separatrix Γ (i.e. at $r=1$):

$$H^{(In)}|_\Gamma = H^{(Ex)}|_\Gamma, \quad \Psi^{(In)}|_\Gamma = C, \quad \frac{\partial}{\partial r}\Psi^{(In)}|_\Gamma = \left.\frac{\partial}{\partial r}\Psi^{(Ex)}\right|_\Gamma. \tag{44}$$

Here and below, superscripts (In) and (Ex) are used to distinguish the boundary values of the variables corresponding to the interior and exterior regions, respectively. Conditions (44) along with (35) secure the continuity of the layer thickness, streamfunction and velocity. As may be seen from (11), these conditions also guarantee the continuity of the Bernoulli function at Γ. Of course, the tangential derivative of H at the separatrix is continuous. Moreover, the radial (normal to Γ) derivative of h is also continuous at the contour Γ. This follows from (43) since, in view of (35) and (44), at the separatrix, $\partial\Psi/\partial\theta = \partial^2\Psi/\partial\theta^2 = 0$ and $\partial\Psi/\partial r$ is continuous.

The term '*smooth solutions*' will be used to designate solutions where PV is continuous everywhere on the (x, y)-plane, including the separatrix Γ. In principle, a constant jump of PV across the separatrix can exist, being a function of $\Psi|_\Gamma = C$. A smooth solution is found by varying parameter C. According to (25), the condition of continuity of P at the separatrix is equivalent to the condition $\mathrm{d}F(\Psi^{(In)})/\mathrm{d}\Psi^{(In)} = \mathrm{d}F(\Psi^{(Ex)})/\mathrm{d}\Psi^{(Ex)}$ at $\Psi^{(In)} = \Psi^{(Ex)} = C$. Owing to (8), the latter means that, in a smooth modon, the Bernoulli function is continuously differentiable, i.e. smooth. Smooth solutions are of the utmost interest because of their potential stability (Kizner *et al.* 2003*a*, *b*). Therefore, in § 5, only smooth modon solutions are presented.

4. Numerical implementation

4.1. *Successive-linearization iterative procedure*

To solve the exterior problem (33)–(36) and interior problem (42)–(44), we adopt a successive linearization (Newton–Kantorovich) iterative procedure and a collocation method with Fourier–Chebyshev spectral representation of h and Ψ. For the construction of modon solutions in classical two-dimensional hydrodynamics, this approach was first used by Boyd & Ma (1990); the theory and applications of Fourier–Chebyshev polynomials are described in detail by Boyd (2001). In the same way as was done by Kizner *et al.* (2003*a*, *b*) and Khvoles *et al.* (2005), the volume of computations will be reduced by assuming the symmetry about the y-axis of the solutions sought:

$$h(x, y) = h(-x, y), \quad \Psi(x, y) = \Psi(-x, y). \tag{45}$$

For this reason, h and ψ are approximated by truncated Fourier–Chebyshev series, or polynomials, as

$$\sum_{0 \leqslant n+2m \leqslant N-1} T_n(r) a_{m,n} \cos(2m\theta) + \sum_{0 \leqslant n+2m \leqslant N-2} T_n(r) b_{m,n} \sin[(2m+1)\theta], \tag{46}$$

where $n \geqslant 0$ and $m \geqslant 0$ are integers, $T_n(r)$ is an n-degree Chebyshev polynomial in r, and $N-1$ is the highest allowed degree.

There are at least two options for dealing with the exterior semi-infinite region. The first way is using the so-called 'shifted Chebyshev polynomials' defined on a finite interval $[1, R]$ with $R \gg 1$. (The term 'shifted' is conventionally used when r ranges in an interval different from $[-1, 1]$.) An alternative way is to use the so-called 'rational Chebyshev polynomials' defined on a semi-infinite interval $[1, \infty)$ and based on rational functions of r. In spite of the exponential decay of the exterior solution at infinity, both modes are appropriate to handle the problem in a finite sub-domain $1 < r \leqslant R$ of the semi-infinite (in r) exterior region (cf. Boyd 2001). By trial, the second mode was chosen, because it leads to somewhat more accurate results, in particular, to a better estimate of $\partial\Psi/\partial r$ at $r = 1$ (accuracy criteria are discussed in § 4.2 and also in § 5.1). Rational Chebyshev polynomials satisfy conditions (36) automatically. Thus, we require fulfilment of the boundary condition (35) only. In the interior domain, shifted Chebyshev polynomials are employed defined on the interval [0, 1].

The Newton–Kantorovich iterative procedure, in essence, consists in the following. Let $i \leqslant NI$ be the iteration index and NI, the number of iterations (tolerance). At the beginning of computations, at $i = 0$, the initial guess of the solution sought, i.e. the pair of functions h_0 and Ψ_0, is specified and approximated in the form (46). Once

approximation i is known, the next approximation, $i+1$, is given by

$$\Psi_{i+1} = \Psi_i + \varphi, \quad h_{i+1} = h_i + \eta, \tag{47}$$

where, the corrections φ and η are supposed to be small relative to Ψ_i and h_i, respectively. For the exterior flow, these corrections must satisfy the inhomogeneous linear equations obtained by substitution of (47) into (33) and (34) and by linearization of the resulting equations with respect to φ and η. Accordingly, when dealing with the interior, equations, (42) and (43) are linearized. Boundary conditions (35) and (44) must be written in terms of φ and η as well.

Theoretically, the Newton–Kantorovich procedure applied to a nonlinear operator equation converges if the operator satisfies some smoothness conditions, and the initial guess is chosen close enough to the solution sought. The convergence is apparent in that the free terms in the linear equations tend to zero as i goes to infinity. The results of our computations presented below demonstrate that, normally (where the existence of a solution is expected), this procedure supplemented with the Fourier–Chebyshev approximation and collocations also converges. In fact, we run two procedures, one for the exterior and the other for the interior domain. As soon as the first procedure converges and the exterior solution is found, boundary conditions (44) for the interior problem are determined.

Preliminary runs have shown that, because of the use of polar coordinates, the accuracy of computation of Q in the near vicinity of the origin ($r=0$) is relatively low. To improve the situation, we supplement the pair of linearized equations (42) and (43) for the interior domain by the linearized version of (14). This system of three equations is consistent, because (14) is a corollary of (42) and (43). Numerically, such an addition suppresses the unwanted effects in the vicinity of the origin, making the errors in this domain of the same order as everywhere in the circle $r \leqslant 1$.

We start by constructing a solution under the conditions which are quite close to those of the quasi-geostrophic approximation. Namely, we set $\Lambda \sim 1$ and $\varepsilon \ll 1$ and, as the initial guess, use a free-surface quasi-geostrophic dipolar modon solution given by (30) and (31). Then, gradually increasing ε, we use the previously found solution as an initial guess for the next solution. This is done for Λ ranging from 0.5 to 5.

4.2. *Collocation and accuracy*

To solve the linear problems formulated above, we apply the collocation method, i.e. require the fulfilment of the equations and boundary conditions in a finite set of external, internal and boundary points. The numbers of grid nodes in the exterior and interior regions are set the same. Owing to the symmetry of the solution about the y-axis, only the right half-plane is considered. To discretize the problem, we cover both the exterior and interior regions with M radial rays ($M > N$) uniformly distributed in the range $-\pi/2 \leqslant \theta \leqslant \pi/2$; the set of rays contains those at which all the functions $\cos(2m\theta)$ and $\sin(2m+1)\theta$ are orthogonal in the discrete sense. Along each ray, a chain of M nodes is determined, containing the points on which Chebyshev polynomials are orthogonal. All in all we have the same number $K_G = M^2$ of grid nodes in either the exterior and interior regions. In addition, we distribute uniformly K_B points over the separatrix (again at $-\pi/2 \leqslant \theta \leqslant \pi/2$), setting $K_B > N$. We then consider the two linear equations corresponding to the exterior domain at each point of the exterior grid and also at the boundary points, thus obtaining a system of $2(K_G + K_B)$ equations. Along with the boundary condition imposed on φ at K_B boundary points, we arrive at a system of $2K_G + 3K_B$ linear equations for the exterior region. Because the number of unknown polynomial coefficients is $N(N+1)$ (see (46)), the total number of equations

NI	RMS Res Eq	Max Res Eq	RMS Res B	Max Res B
1	0.0251	0.0138	5.80×10^{-8}	1.10×10^{-7}
2	1.30×10^{-4}	6.85×10^{-4}	3.55×10^{-8}	9.40×10^{-8}
3	6.19×10^{-7}	2.98×10^{-6}	1.34×10^{-9}	2.07×10^{-9}
4	6.19×10^{-7}	2.97×10^{-6}	1.29×10^{-9}	2.07×10^{-9}

TABLE 1. Accuracy characteristics at the output of the exterior iterative procedure ($\Lambda = 1$, $\varepsilon = R_O = 0.1$). The root-mean-square and maximal residuals in the pair of linearized equations (33) and (34), RMS Res Eq and Max Res Eq, and in the fulfilment of boundary condition (35), RMS Res B and Max Res B.

NI	RMS Res Eq	Max Res Eq	RMS Res B	Max Res B
1	0.0921	2.744	0.0269	0.0481
5	4.43×10^{-5}	3.13×10^{-4}	6.19×10^{-5}	1.11×10^{-4}
10	5.98×10^{-6}	3.121×10^{-5}	1.58×10^{-5}	2.93×10^{-5}
15	3.56×10^{-6}	2.164×10^{-5}	1.23×10^{-5}	1.87×10^{-5}
20	3.47×10^{-6}	2.011×10^{-5}	1.21×10^{-5}	2.01×10^{-5}

TABLE 2. Accuracy characteristics at the output of the interior iterative procedure ($\Lambda = 1$, $\varepsilon = R = 0.1$). The root-mean-square and maximal residuals in the pair of linearized equations (42) and (43), RMS Res Eq and Max Res Eq, and in the fulfilment of boundary conditions (44), RMS Res B and Max Res B.

exceeds the number of unknowns. The matrix of this overdetermined linear system and the vector of free coefficients (residuals) depend on the iteration index i. At each iteration step, this linear system is solved in the least-squares sense. In a similar way, when considering the interior domain, we obtain $3K_G + 6K_B$ linear equations and solve them in the least-squares sense.

We estimate the accuracy of the numerical method based on the following criteria. First, in the scatter-plots of Q *vs.* Ψ and B *vs.* Ψ, the scattering of points must be reasonably small, testifying to the existence of functional dependences of Q and B on Ψ. Secondly the computed derivative of B as a function of Ψ must be close to the apparent functional dependence of P on Ψ. Thirdly at the end of the iterative process, the residuals must be sufficiently small.

The accuracy of the computational procedure is a function of its parameters: the radius R of the circle chosen for computations, the number K_G of grid nodes (in the interior and exterior regions), the number of boundary points, K_B, the polynomial degree, N, and the number NI of iterations made (tolerance). It also depends on the physical parameters Λ and ε of the problem. The stronger the ageostrophicity, the lower the accuracy; this conclusion is valid if all other parameters are fixed. At a fixed Λ, the accuracy decreases with increasing ε. At given Λ and ε, the accuracy generally increases with increasing number of iterations NI.

Through the boundary conditions, the errors present in the exterior solution influence the accuracy at which the interior problem is solved. Thus, good convergence of the exterior procedure is essential for the good quality of both the exterior and interior solutions. A different number of iterations, NI, is required for a reasonable convergence in the interior and exterior domains. In the exterior procedure, the errors decrease considerably when NI is increased from 1 to 3, and less rapidly when it is increased from 3 to 5 (table 1). In the interior procedure, the errors decrease quite rapidly during the first 15 iteration steps, and less rapidly when NI is increased from

15 to 20 (table 2). In the headings of tables 1 and 2, the following notations are used: RMS Res Eq is the root-mean-square residual in the right-hand side of linear equations for the exterior or interior domain at the output of the iterative process; Max Res Eq, the corresponding maximum absolute residual. Analogously, RMS Res B and Max Res B denote the residuals in the fulfilment of the boundary condition for the exterior and interior solutions.

Our tests show that satisfactory results are obtained with the following parameters: $R=6$, $M=50$, $K_B=300$, $N=14$. The tolerance, NI, is fixed as 7 for the exterior procedure, and 20 for the interior procedure. These parameters fitted by trial at the stage of tuning the model are used to compute all the solutions presented below.

5. Results and discussion

5.1. *Modon characteristics and accuracy estimates*

The central question of our work is whether the RSW modon solutions exist. Employing the method described in §4, we managed to construct the solutions with required properties. These modon solutions satisfy equations (19)–(21) to within small errors and exist in some domain of the three-dimensional parameter space (Λ, ε, C).

As mentioned above (§3.4), in general, the PV in an RSW modon solution is continuous everywhere on the (x, y)-plane, except the separatrix. Along the separatrix, the interior and exterior PV is constant, but across the separatrix, a jump of P may occur. At a given pair Λ, ε this jump, $[P]_\Gamma = Ro[Q]_\Gamma = Ro(Q^{(Ex)}|_\Gamma - Q^{(In)}|_\Gamma)$, depends on parameter C that appears in boundary conditions (35) and (44). Our computations reveal that (at least for dipolar solutions) $[P]_\Gamma$ is a monotonic function of C that, for a continuum of pairs (Λ, ε), changes the sign. Thus, for each pair (Λ, ε) within a certain domain in the (Λ, ε)-plane, a unique smooth dipolar modon solution exists, determined by a particular C. In other words, the family of smooth circular RSW modons is two-parameter: the non-dimensional parameters determining a modon are Λ and ε, and the corresponding dimensional parameters are L and U. Below, only smooth solutions are discussed.

Once the question of existence of RSW modons is answered positively, the key questions become the following.

(i) How does deviation from quasi-geostrophicity affect the modon structure for a spectrum of modon sizes and translation speeds?

(ii) What values of L and U (or Λ and ε) permit the existence of smooth modon solutions?

To answer these questions, we ran computations with different combinations of the values of Λ and ε. Condition (40) stating that an RSW modon must propagate more slowly than inertia–gravity waves, poses the theoretical upper bound to the translation speed of any modon. One may anticipate that the conditions for the existence of smooth modons will impose an even stronger restriction on the translation speed. Therefore, in the context of question (ii), it will be only natural to interpret our results in terms of the translation speed normalized with the phase speed of gravity waves, $\tilde{U} = U/\sqrt{g'H_0}$. Clearly, the non-dimensional parameter $\tilde{U}$ can be expressed in terms of Λ and ε, or Λ and Ro; namely, $\tilde{U} = \varepsilon/\Lambda = Ro\Lambda$.

The main results are summarized in figures 1–6 (all variables are non-dimensional). Figures 1–3 represent three f-plane RSW smooth modons of the same size $\Lambda = 1$ at $Ro = \varepsilon = \tilde{U} = 0.04$, 0.12, 0.2. In all cases, the modon consists of two vortices, a cyclone and anticyclone. The cyclone is characterized by a larger peak absolute value

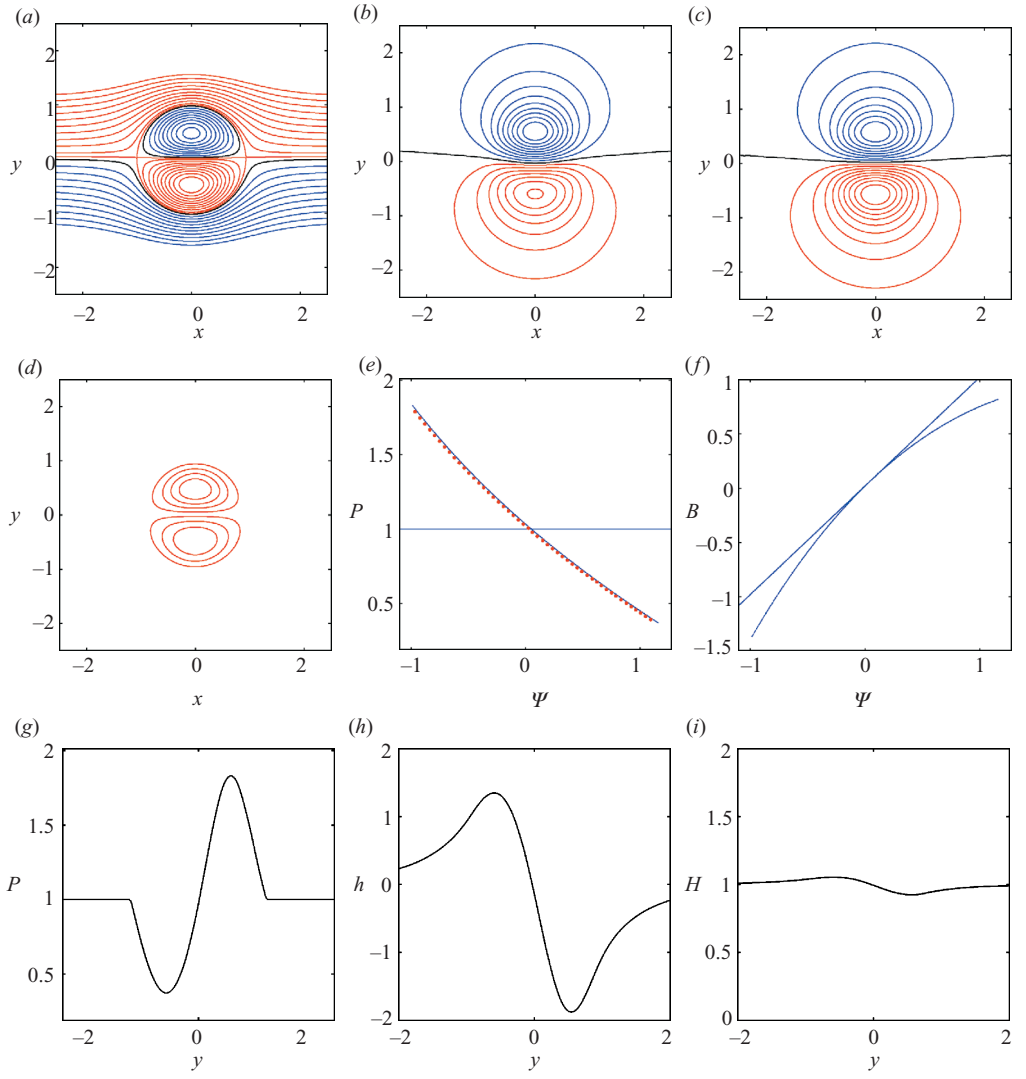

FIGURE 1. Characteristics of the smooth modon solution at $\Lambda = 1$ and $Ro = \varepsilon = \tilde{U} = 0.04$ ($C \approx 0.05357$). (*a*) Contours of the co-moving streamfunction Ψ; (*b*) contours of the layer thickness deviation h; (*c*) contours of $\psi = \Psi - y$; (*d*) contours of PV; (*e*) PV *vs.* Ψ scatter-plot; (*f*) B *vs.* Ψ scatter-plot; (*g*) cross-section of PV along the y-axis; (*h*) cross-section of h along the y-axis; (*i*) cross-section of the layer thickness, $H = 1 + \varepsilon h$, along the y-axis. Iso-contours in (*a*)–(*d*) are given at a 10%-step of the maximum; black line, zero contour. In (*e*) and (*f*), the straight blue lines correspond to the exterior region, and the curved blue lines, to the interior. The chain of red points in (*e*), interior $\mathrm{d}B/\mathrm{d}\Psi$ *vs.* Ψ relation (computed by a direct numerical differentiation of the function $B(\Psi)$).

of PV and a stronger deviation of the active-layer thickness from the ambient level. Figures 4 and 5 represent the peak values of the modon PV in the cyclone, P_{max}, and the minimal layer thickness, H_{min}, respectively, as functions of $\tilde{U}$ at different Λ. In figure 6, the domain on the $(\tilde{U}, \Lambda)$-plane is shown, where the modon solutions exist. Note that, at $\Lambda = 1$, the modon radius is equal to the Rossby deformation radius L_R (which appears relevant to mesoscale eddies in the ocean and atmosphere), while

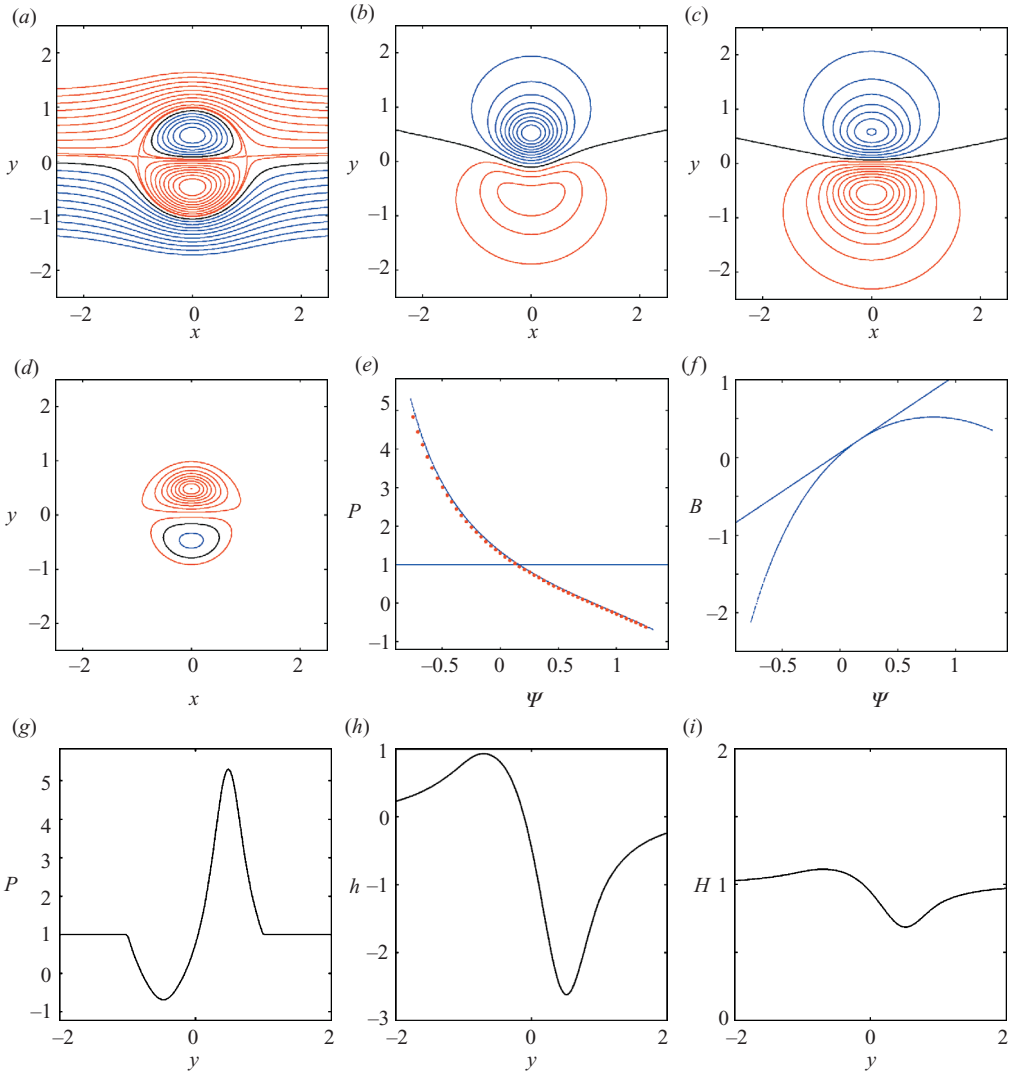

FIGURE 2. Characteristics of the smooth modon solution at $\Lambda = 1$ and $Ro = \varepsilon = \tilde{U} = 0.12$ ($C \approx 0.16232$). Notations as in figure 1.

setting, for example, $\Lambda = 0.5$ or 2 means that the modon radius is half the size or twice as big as L_R.

A reliable verification of the accuracy, at which the modon solutions is obtained, is provided by scatter-plots of P *vs.* Ψ and B *vs.* Ψ A visual indication of relatively high accuracy achieved with the use of our numerical method is that the points (P, Ψ) and (B, Ψ) in the scatter-plots (figures 1*e*, *f*, 2*e*, *f*, and 3*e*, *f*) cluster densely around the straight lines that represent the exterior solution, and around the curved lines representing the interior solution. As predicted by the theory ((24) and (25)), the graph of function $\mathrm{d}B/\mathrm{d}\Psi$ fits well that of $P(\Psi)$ (figures 1*e*, 2*e*, 3*e*). The derivative is computed by dividing the range of Ψ values into a number of small equally long intervals, calculating the mean values of B and Ψ for the points (B, Ψ) falling into each interval, and estimating the derivative at the end of each interval as the ratio of differences of neighbouring means. In terms of the scatter-plots, the smoothness

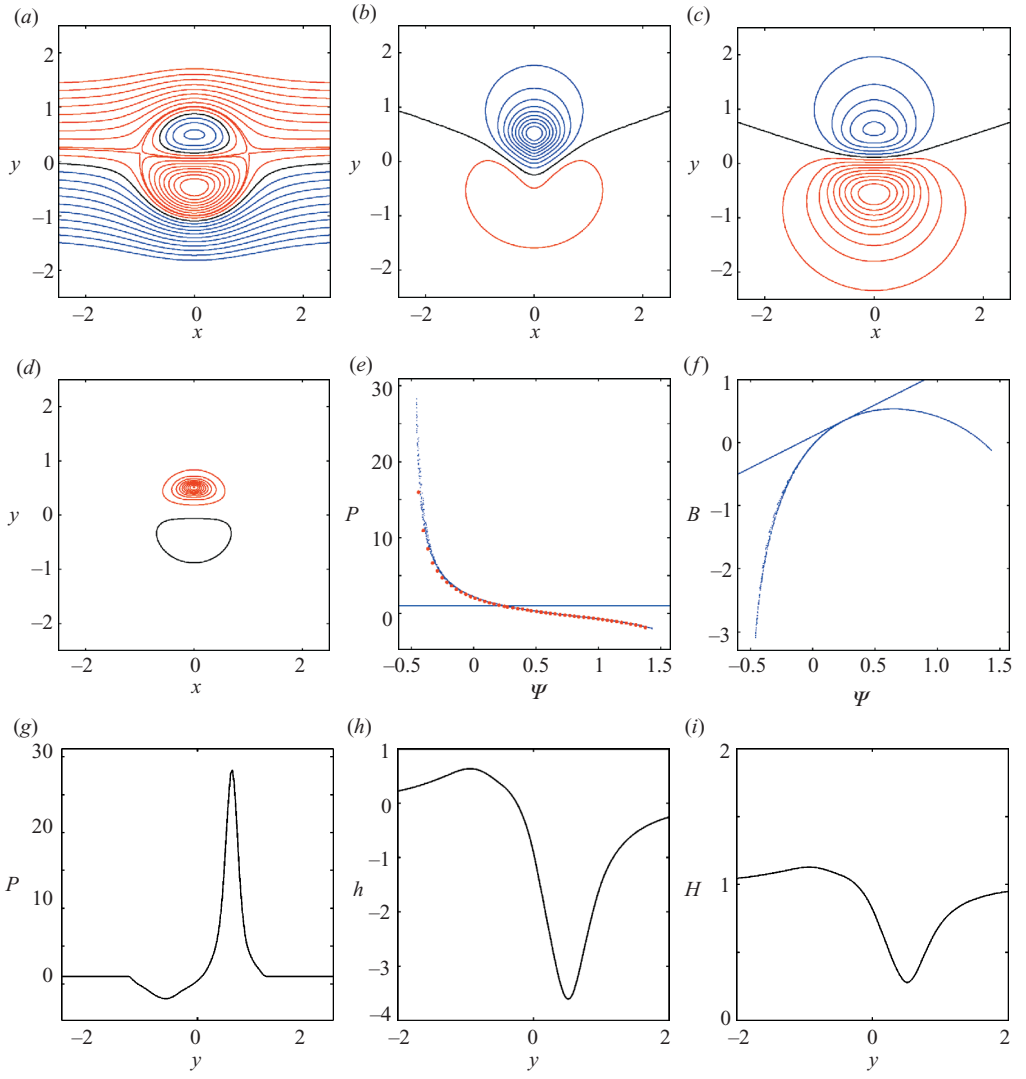

FIGURE 3. Characteristics of the smooth modon solution at $\Lambda = 1$ and $Ro = \varepsilon = \tilde{U} = 0.2$ ($C \approx 0.25170$). Notations as in figure 1.

of the solutions found is evidenced by the fact that, in figures $1f$, $2f$ and $3f$, the straight lines representing the B *vs.* Ψ dependence in the exterior region are apparently tangent to the curved lines representing this dependence in the interior region. The continuity of the PV field can also be judged from the PV cross-sections shown in figures $1g$, $2g$ and $3g$. Regarding the integral mass anomaly which is supposed to be zero (§ 2.3), the accuracy is also reasonable. In fact, while the two integrals of $|h|$ over the areas, where h is positive and negative, are of the order of 1 each, the difference between the two integrals ranges approximately from 0. 04% (at $\varepsilon = Ro = 0.04$) to 3% (at $\varepsilon = Ro = 0.2$) of the overall integral of $|h|$. Yet, it is as well to bear in mind that, in spite of the fast decrease of h at infinity, the far field may contribute considerably to the integral mass anomaly (and, as figures $1h$–$3h$ show, the larger $\varepsilon = Ro$, the stronger this contribution in the anticyclone mass anomaly). Therefore, the modon mass anomaly might be expected to be sufficiently close to zero only if computed

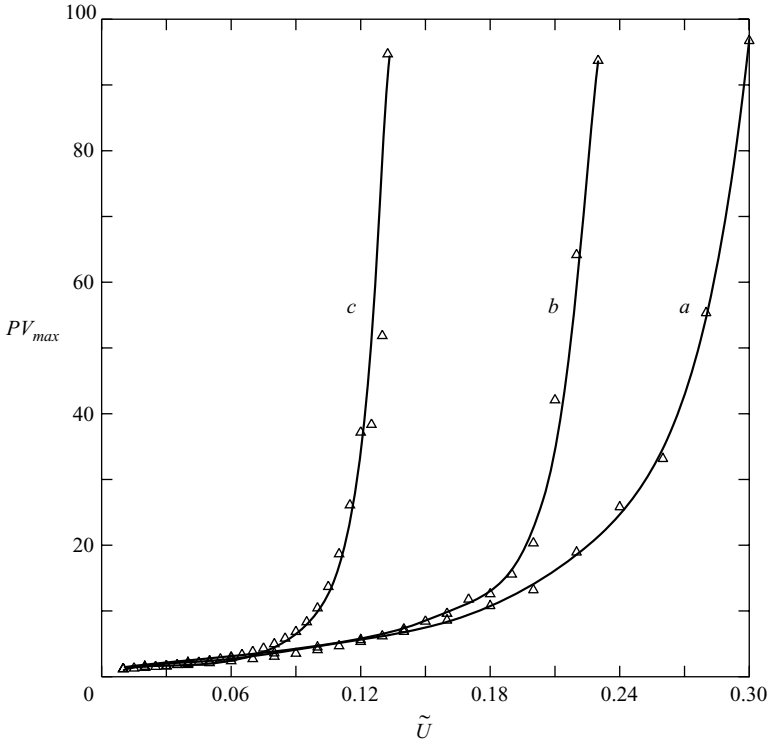

FIGURE 4. Peak values of PV *vs.* $\tilde{U}$. *a*, $\Lambda = 0.5$; *b*, $\Lambda = 1$; *c*, $\Lambda = 2$.

ε	Mean Res Exterior	Mean Res Interior	Mean (Ψ)	Mean (h)	Mean ($\partial\Psi/\partial r$)	Mean (P)
0.04	5.90×10^{-7}	9.64×10^{-5}	4.22×10^{-6}	1.05×10^{-5}	1.14×10^{-4}	3.16×10^{-5}
0.12	6.10×10^{-7}	1.73×10^{-4}	2.72×10^{-4}	2.50×10^{-4}	1.52×10^{-3}	1.14×10^{-3}
0.20	1.91×10^{-6}	9.64×10^{-4}	3.86×10^{-3}	2.01×10^{-3}	8.36×10^{-3}	1.24×10^{-2}

TABLE 3. Accuracy characteristics of the solutions shown in figures 1–3 ($\Lambda = 1$). The root-mean-square residuals in the fulfilment of equations in the exterior and interior domains (first two columns) and discrepancies in the fulfilment of boundary conditions at the separatrix.

over a appreciably larger area on the (x, y)-plane. We, however, construct numerical solutions in a circle $r \leqslant 6$, which makes impossible a genuine estimation of the overall mass anomaly. Some additional accuracy estimates for the solutions shown in figures 1–3 are provided in table 3.

5.2. *Size and speed dependence and a solvability bound*

At relatively small values of $Ro = \varepsilon$ and, hence, of $\tilde{U}$ (figure 1) the ageostrophic effects are small. Therefore, the solution obtained appears similar to a quasi-geostrophic modon, (30) and (31). The layer-thickness deviation h and streamfunction fields ψ and Ψ are nearly anti-symmetric relative to the x-axis (figure 1 *a–c*, *h*, *f*), the contours of h and ψ being almost identical (figure 1*b*, *c*). The relative thickness deviation εh is small (figure 1*i*), and nonlinearity of the interior PV *vs.* Ψ relation is weak (figure 1*e*). The latter corresponds well with the recent finding (Kizner *et al.*

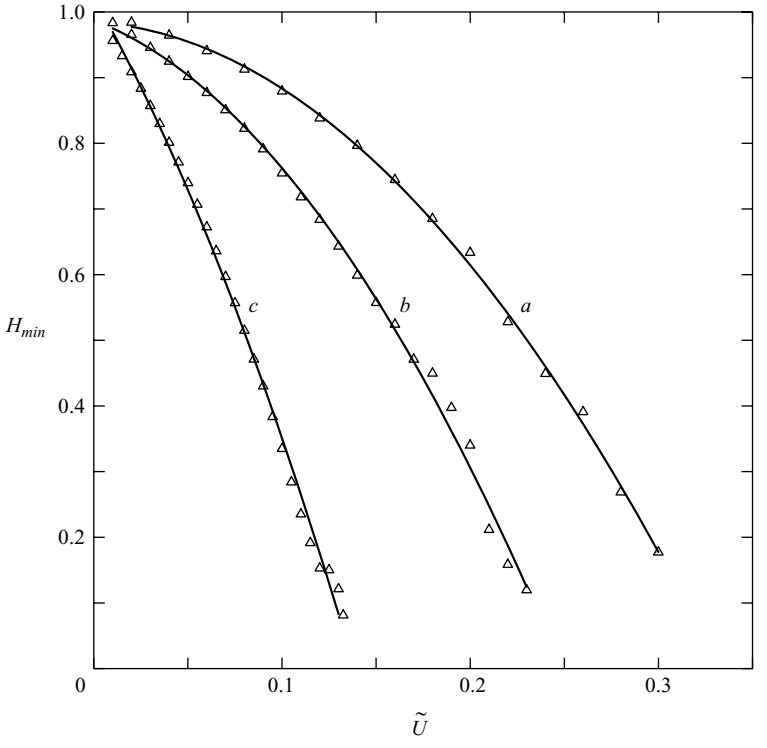

FIGURE 5. Minimal layer thickness, H_{min}, *vs.* $\tilde{U}$. *a*, *b*, *c*, as in figure 4.

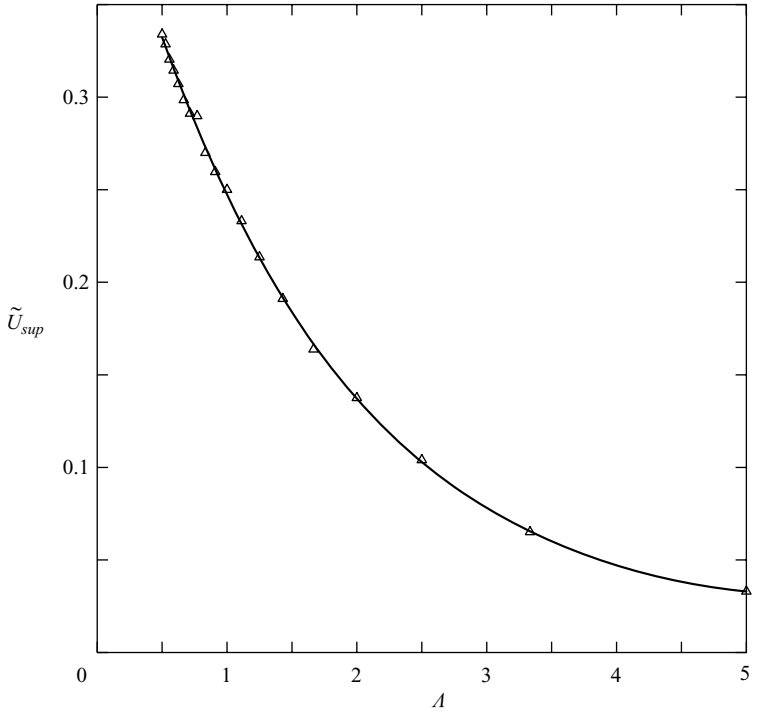

FIGURE 6. The upper bound of the translation speeds of smooth modons, $\tilde{U} = \tilde{U}_{sup}(\Lambda)$.

2003*a*, *b*; Khvoles *et al.* 2005) that, in the quasi-geostrophic approximation (or in classical two-dimensional hydrodynamics), circularity of the separatrix and linearity of the interior PV *vs.* Ψ relation are equivalent properties of a modon.

Comparison of figures 1–3 shows that growing ageostrophicity, resulting from the increase of *Ro* (i.e. of $\tilde{U}$) at a fixed Λ, destroys the antisymmetry of the solution about the x-axis. The difference between the h- and ψ-fields, as well as the nonlinearity of the interior PV *vs.* Ψ relation, increases. The amplitudes of variation of the layer thickness H in each vortex grow, the peak value of $|h|$ in the cyclone being larger than that in the anticyclone. Accordingly, to keep the mass anomaly zero (see (18)), the anticyclone expands and the cyclone contracts with increasing $\tilde{U}$. Thus, in terms of PV, one of the two vortices constituting the modon, the cyclone, enhances while the layer thickness in this vortex decreases.

Qualitatively, the difference between the cyclone and anticyclone in an RSW vortex pair can be explained by considering a stationary axisymmetric vortex, a cyclone or anticyclone, which is in the gradient–wind balance (see also Konshin & Shapiro 1988):

$$f v_\theta + \frac{v_\theta^2}{r} = g' \frac{\partial h}{\partial r}. \tag{48}$$

Here, v_θ is the azimuthal velocity in polar coordinates with the origin in the centre of the vortex; (48) can be derived from (1), (2). From (48) it follows that, if a cyclone and anticyclone are antisymmetric in terms of h, the revolution of fluid particles in the anticyclone is faster than in the cyclone. This is because, in the cyclone, v_θ and $\partial h/\partial r$ are both positive, while in the anticyclone they are negative. [In terms of geostrophic adjustment, the cyclone–anticyclone asymmetry was demonstrated by Kuo & Polvani (2000). Based on conservation laws and using numerics, they showed that equally strong circular pressure or velocity anomalies, whose profiles differ only in sign, adjust in such a way that a balanced cyclone is stronger than the anticyclone. Asymmetry between large-scale RSW cyclones and anticyclones was also observed experimentally in the wakes past obstacles dragged in the upper layer of a two-layer fluid (Perret *et al.* 2006).] Thus, as distinct from the QG approximation, if an RSW pair cyclone–anticyclone were initially antisymmetric, the anticyclone would have been propelling its counterpart faster than the cyclone. To put it differently, an RSW dipole can propagate uniformly along a straight line only when the pressure (active-layer thickness) profile in the cyclone slopes more sharply than in the anticyclone.

The tendencies revealed in the above discussion (figures 1–3) are confirmed by computations in broad ranges of parameters $\tilde{U}$ and Λ. An informative characteristic of an RSW modon is the peak value of PV, P_{max}, which is assumed at the centre of the cyclonic vortex (figures 1*e*, *g*–3*e*, *g*). A typical behaviour of the PV maximum as a function of $\tilde{U}$ is presented in figure 4, where a monotonic increase of P_{max} at a given Λ and growing $\tilde{U}$ can be observed. Moreover, a characteristic feature of RSW modons is that also $\partial P_{max}/\partial \tilde{U}$ increases monotonically (unlike QG modons, in which the PV maximum depends linearly on the translation speed). If, on the other hand, two modons propagate at the same speed, then the modon with a larger radius has a larger P_{max}. That is to say, of two modons of different size, the larger modon should have a larger P_{max} in order to move with the same speed as the smaller modon.

The intensification of the cyclonic vortex with increasing $\tilde{U}$ at a fixed Λ is associated with a decrease in the minimal layer thickness, H_{min}, in this vortex. Such a behaviour of H_{min} is demonstrated in figure 5. As expected, the cyclone in a larger modon is shallower than the cyclone in a smaller modon at the same speed $\tilde{U}$. An important

point is that H_{min} rapidly decreases with increasing $\tilde{U}$. This suggests that, for a fixed Λ, at a certain $\tilde{U} = \tilde{U}_{sup}(\Lambda)$, the layer thickness will vanish, while P_{max} will go to infinity as $\tilde{U} \to \tilde{U}_{sup}$. The monotonic character of function $H_{min} = H_{min}(\tilde{U})$ along with the fact that the problem set-up is relevant only for positive H lead us to the conjecture that smooth modon solutions can exist only within the interval $0 < \tilde{U} < \tilde{U}_{sup}(\Lambda)$.

The results of our computations support the above conjecture. The upper bound of the allowed $\tilde{U}$-values is estimated in the following way. In fact, growing gradients of P limit our ability to perform computations with $\tilde{U}$ which is too close to $\tilde{U}_{sup}(\Lambda)$. Therefore, for each fixed Λ, we construct smooth solutions at gradually increasing ε (i.e. increasing $\tilde{U}$) until $\tilde{U}$ reaches the maximal available value $\tilde{U}_M$; the values of H_{min} corresponding to $\tilde{U}_M$ are positive but rather small (figure 5). Next we extrapolate function $H_{min}(\tilde{U})$ to the point where it vanishes, and choose the corresponding value of $\tilde{U}$ in the capacity of $\tilde{U}_{sup}(\Lambda)$. The resulting curve $\tilde{U} = \tilde{U}_{sup}(\Lambda)$ is shown in figure 6. It is obvious that $\tilde{U}_{sup}(\Lambda)$ monotonically decreases with increasing Λ, i.e. the bigger the modon the narrower the range of allowed translation speeds. The largest value of $\tilde{U}_{sup}(\Lambda)$ in figure 6 is reached at $\Lambda = 0.5$ (the smallest modon radius to which the computations were run) and is approximately equal to 0.33. Thus, as expected, for all smooth modon solutions found, the condition of non-negative thickness of the active layer, $0 < \tilde{U} < \tilde{U}_{sup}(\Lambda)$, proves to be much more restrictive than the non-radiation condition (40) which requires only that $0 < \tilde{U} \leqslant 1$.

6. Conclusion

This work has extended the family of modon solutions to the f-plane RSW model. As with QG modons, there is a separatrix in an RSW modon. In a frame of reference co-moving with the modon, the separatrix is the closed streamline demarcating the interior (trapped-fluid) region, where the streamlines are closed, from the exterior region, where the fluid passes around the modon. Although, in RSW modons, a PV jump across the separatrix is allowed, our main effort went into the search for smooth modons. A smooth RSW modon is distinguished by the continuity of its PV and smoothness of velocity, pressure gradients, and energy as functions of x and y. Such a modon normally appears as a pair of vortices of different rotation, a cyclone and an anticyclone. In a fixed frame of reference, the velocity field associated with the modon falls off exponentially at $r \to \infty$. Thus, in fact, we are dealing with two-dimensional solitons.

The total mass anomaly of an RSW modon is defined as the integral (over the (x, y)-plane) deviation of the active-layer thickness from its ambient value. Just as in QG modons, the mass anomaly of an RSW modon is zero. At the same time, ageostrophic factors endow an RSW modon with new properties. First, unlike the QG model, the f-plane RSW model permits inertia–gravity waves; therefore, to preserve its parameters, i.e. to ensure the lack of wave radiation, an RSW modon has to propagate more slowly than these waves. In other words, the modon translation speed $U$is bounded from above by the phase speed of gravity waves, $\sqrt{g'H_0}$. Secondly, in the RSW modons with circular separatrices, the PV *vs.* Ψ relation is nonlinear in the trapped-fluid area, whereas in QG circular modons it is necessarily linear. Thirdly, the cyclone and anticyclone constituting an RSW modon have different form and intensity, whereas in a QG modon, the cyclone and anticyclone are anti-symmetric (i.e. differ only in sign). In an RSW modon, the cyclone is more intense and compact than the anticyclone; the variation of the active-layer thickness and, therefore, the peak PV in the cyclone are larger than in the anticyclone (in absolute value). Importantly, the minimal layer thickness in the cyclone rapidly decreases with increasing U at a given

modon radius L and vanishes at a certain speed. This imposes a more restrictive condition on the allowed translation speed of a smooth modon, $U < U_{sup}(L)$. The upper bound of the translation speed, $U_{sup}(L)$, monotonically decreases with increasing radius L and is appreciably smaller than the phase speed of gravity waves, $\sqrt{g'H_0}$. For example, at $L = 0.5L_R$ (the minimal modon radius considered in our computations), the boundary value $U_{sup}(L)$ is under $0.33\sqrt{g'H_0}$.

The modon solutions were sought numerically using the Newton–Kantorovich iterative technique. Our approach comprising a few stages has some specific features enabling an effective search for smooth solutions. First, we prescribe the modon separatrix (a circle of radius L in our case), the translation speed U, and the constant value C of the streamfunction at the separatrix. Next we set the pair of equations that govern the exterior flow and require constancy of PV and linearity of the energy–streamfunction relation. This exterior problem is solved with the use of Fourier–Chebyshev polynomials and a Newton–Kantorovich procedure with collocation for calculation of the polynomial coefficients. Given the exterior solution, the boundary conditions for the interior solution at the separatrix are fully determined. This allows the construction of the interior solution in a procedure similar to that used for the exterior domain, but based on the original equations for a stationary flow in a co-moving frame of reference. At given U and L, the family of modon solutions depends on the single parameter C. By varying C, we arrive at the unique smooth modon solution. Our results demonstrate the potency of this technique. By using elliptic coordinates it can be extended to the search for modons with elliptical separatrices (cf. Boyd & Ma 1990; Kizner *et al.* 2003*a*). We can anticipate that among elliptical modons (that depend on four non-dimensional parameters Λ, ε, C, and the ellipse aspect ratio), the so-called supersmooth modons can exist, categorized by the smoothness of the PV field (cf. Khvoles *et al.* 2005). The methodological ideas underlying this approach can be applied to seeking RSW modons on the β-plane or in spherical geometry. They may also be applied, in later stages, to the search for truly three-dimensional modon solutions of primitive equations.

As for the smooth f-plane RSW modons presented in this paper, we believe that the next step should be testing of their stability in a numerical model with forward integration in time. At small Rossby numbers, because of the geostrophic splitting, a balanced solution will be stable relative to inertia–gravity waves in the sense that, although a small perturbation will cause radiation of waves, the energy of the radiated signal will remain small (e.g. Reznik, Zeitlin & Ben Jelloul 2001). However, for Rossby numbers of the order of 1 it may not be the case. A question that can be asked in this context is: If an RSW modon is unstable, will it disintegrate when subjected to a small initial perturbation, or will it radiate inertia–gravity waves and, eventually, adjust to a new balanced state?

This research was supported by the Israel Science Foundation grant 628/06 and the Binational Israel–US Science Foundation (BSF) grant 2002392. G.R. acknowledges the support from the Russian Foundation for Basic Research grant 08-05-00006. The authors are indebt to T. Smirnov for help with writing the Matlab code. The anonymous referees are thanked for helpful comments on the manuscript.

REFERENCES

Berestov, A. L. 1979 Solitary Rossby waves. *Izv. Acad. Sci. USSR. Atmos. Ocean Phys.* **15**, 648–654.

Berestov, A. L. 1981 Some new solutions for the Rossby solitons. *Izv. Acad. Sci. USSR. Atmos. Ocean. Phys.* **17**, 82–87.

Boyd, J. P. & Ma, H. 1990 Numerical study of elliptical modons using spectral methods. *J. Fluid Mech.* **221**, 597–611.

Boyd, J. P. 2001 *Chebyshev and Fourier Spectral Methods,* 2nd edn, Dover.

Chaplygin, S. A. 1903 One case of vortex motion in fluid. *Trans. Phys. Sect. Imperial Moscow Soc. Friends of Natural Sciences* **11** (N 2) 11–14.

Flierl, G. R., Larichev, V. D., McWilliams, J. C. & Reznik, G. M. 1980 The dynamics of baroclinic and barotropic solitary eddies. *Dyn. Atmos. Oceans* **5**, 1–41.

Flierl, G. R., Stern, M. E. & Whitehead Jr, J. A. 1983 The physical significance of modons: laboratory experiments and general integral constraints. *Dyn. Atmos. Oceans* **7**, 233–263.

Flór, J. B. & van Heijst, G. J. F. 1994 An experimental study of dipolar vortex structures in a stratified fluid. *J. Fluid Mech.* **279**, 101–133.

Haupt, S. E., McWilliams, J. C. & Tribbia, J. J. 1993 Modons in shear flow. *J. Atmos. Sci.* **50**, 1181–1198.

Hesthaven, J. S., Lynov, J. P., Nielsen, A. H., Rassmussen, J. J., Schmidt, M. R., Shapiro, E. G. & Turitsyn, S. K. 1995 Dynamics of a nonlinear dipole vortex. *Phys. Fluids* **7**, 2220–2229.

Khvoles, R., Berson, D. & Kizner, Z. 2005 The structure and evolution of barotropic elliptical modons. *J. Fluid Mech.* **530**, 1–30.

Khvoles, R., McWilliams, J. C. & Kizner, Z. 2007 Non-coincidence of separatrices in two-layer modons. *Phys. Fluids* **19**, 056602/1–14.

Kizner, Z. 1984 Rossby solitons with axisymmetric baroclinic modes. *Dokl. USSR Acad. Sci.* **275**, 1495–1498.

Kizner, Z. 1986*a* Strongly nonlinear solitary Rossby waves. *Oceanology* **26**, 382–388.

Kizner, Z. 1986*b* Intensive synoptic eddies and the quasi-geostrophic approximation. *Oceanology* **26**, 28–35.

Kizner, Z. 1988 On the theory of intrathermocline eddies. *Dokl. USSR. Acad. Sci.* **300**, 453–457.

Kizner, Z. 1997 Solitary Rossby waves with baroclinic modes. *J. Mar. Res.* **55**, 671–685.

Kizner, Z. & Berson, D. 2000 Emergence of modons from collapsing vortex structures on the β-plane. *J. Mar. Res.* **58**, 375–403.

Kizner, Z., Berson, D. & Khvoles, R. 2002 Baroclinic modon equilibria on the beta-plane: stability and transitions. *J. Fluid Mech.* **468**, 239–270.

Kizner, Z., Berson, D. & Khvoles, R. 2003*a* Non-circular baroclinic beta-plane modons: constructing stationary solutions. *J. Fluid Mech.* **489**, 199–228.

Kizner, Z., Berson, D., Reznik, G. & Sutyrin, G. 2003*b* The theory of beta-plane baroclinic topographic modons. *Geophys. Astrophys. Fluid Dyn.* **97**, 175–211.

Konshin, V. N. & Shapiro, G. I. 1988 The evolution of two-dimensional Rossby solitons under the influence of finite amplitude effects. *Dokl. USSR Acad. Sci.* **300**, 1461–1465.

Kuo, A. C. & Polvani, L. M. 2000 Nonlinear geostrophic adjustment, cyclone–anticyclone asymmetry, and potential vorticity rearrangement. *Phys. Fluids* **12**, 1087–1100.

Lamb, H. 1895 *Hydrodynamics*, 2nd edn. Cambridge University Press.

Larichev, V. D. & Reznik, G. M. 1976*a* Two-dimensional solitary Rossby waves. *Dokl. USSR. Acad. Sci.* **231**, 1077–1080.

Larichev, V. D. & Reznik, G. M. 1976*b* Strongly nonlinear two-dimensional solitary Rossby waves. *Oceanology* **16**, 961–967.

Li, C. 2004 A geosolitary wave solution on the f plane. *J. Phys. Oceanogr* **34**, 856–864.

Malanotte-Rizzoli, P. 1982 Planetary solitary waves in geophysical flows. *Adv. Geophys.* **24**, 147–224.

Meleshko, V. V. & van Heijst, G. J. F. 1994 On Chaplygin's investigations of two-dimensional vortex structures in an inviscid fluid. *J. Fluid Mech.* **272**, 157–182.

Neven, E. C. 1994 Baroclinic modons on a sphere. *J. Atmos. Sci.* **51**, 1447–1464.

Nycander, J. 1988 New stationary vortex solutions of the Hasegawa–Mima equation. *J. Plasma Phys.* **39**, 418–428.

Pallas-Sanz, E. & Viudez, A. 2007 Three-dimensional ageostrophic motion in mesoscale vortex dipoles. *J. Phys. Oceanogr.* **37**, 84–105.

Pakyari, A. & Nycander, J. 1996 Steady two-layer vortices on the beta-plane. *Dyn. Atmos. Oceans* **25**, 67–86.

Pedlosky, J. 1987 *Geophysical Fluid Dynamics.* Springer.

Perret, G., Stegner, A., Farge, M. & Pichon, T. 2006 Cyclone–anticyclone asymmetry of large-scale wakes in the laboratory. *Phys. Fluids* **18**, 036603/1–11.

Reznik, G. M. 1992 Dynamics of singular vortices on a beta-plane. *J. Fluid Mech.* **40**, 405–432.

Reznik, G. M. & Sutyrin, G. G. 2001 Baroclinic topographic modons. *J. Fluid. Mech.* **437**, 121–142.

Reznik, G. M., Zeitlin, V. & Ben Jelloul, M. 2001 Nonlinear theory of geostrophic adjustment. Part 1. Rotating shallow-water model. *J. Fluid Mech.* **445**, 93–120.

Sous, D., Bonneton, N. & Sommeria, J. 2004 Turbulent vortex dipoles in a shallow water layer. *Phys. Fluids* **16**(8), 2886–2898.

Stern, M. E. 1975 Minimal properties of planetary eddies. *J. Mar. Res.* **33**, 1–13.

Swenson, M. 1987. Stability of equivalent-barotropic riders. *J. Phys. Oceanogr.* **17**, 492–506.

Tribbia, J. J. 1984. Modons in spherical geometry. *Geophys. Astrophys. Fluid Dyn.* **30**, 131–168.

Verkley, W. T. M. 1984. The construction of Barotropic modons on a sphere. *J. Atmos. Sci.* **41**, 2492–2504.

Verkley, W. T. M. 1987 Stationary barotropic modons in westerly background flows. *J. Atmos. Sci.* **44**, 2383–2398.

Verkley, W. T. M. 1993 A numerical method to find form-preserving free solutions of the barotropic vorticity equation on a sphere. *J. Atmos. Sci.* **50**, 1488–1503.